

Dealloying Behavior of Dual-Phase Al 15 at.% Cu Alloy in an Acidic Solution

Wenbo Liu,^{1,2} Shichao Zhang,^{1,*} Ning Li,² Jiwei Zheng,¹ Shenshen An,¹ and Yalan Xing¹

¹ School of Materials Science and Engineering, Beihang University, Beijing 100191, China

² School of Manufacturing Science and Engineering, Sichuan University, Chengdu 610065, China

*E-mail: liuwenbo_8338@163.com; csc@buaa.edu.cn

Received: 3 November 2011 / Accepted: 31 January 2012 / Published: 1 March 2012

To further understand the underlying physical mechanisms of dealloying of multi-phase alloys, dealloying behavior of melt-spun Al 15 at.% Cu alloy comprising α -Al solid solution and Al₂Cu intermetallic compound in a 5 wt.% hydrochloric acid (HCl) aqueous solution was investigated. The microstructure of as-dealloyed samples was characterized using X-ray diffraction, scanning electron microscopy, energy dispersive X-ray analysis, and transmission electron microscopy. The experimental results show the Al-Cu alloy with the amount of α -Al comparable to that of Al₂Cu can be completely dealloyed, which eventually results in the formation of nanoporous copper (NPC) with a homogeneous porous structure, while during which two other kinds of nanoporous structures can be sequentially obtained for different dealloying times. The formation mechanism has been well established to describe the morphological and compositional evolutions during dealloying process based upon kinetic competitions between dissolution of Al atoms and diffusion-rearrangement of Cu atoms, which includes three stages orderly defined as “ α -Al dealloying,” “Al₂Cu dealloying,” and “coarsening of NPC in porous pore walls.”

Keywords: Dual-phase alloy; Dealloying behavior; Acidic solution; Formation mechanism

1. INTRODUCTION

Nanoporous metals with large surface area have recently attracted considerable interest in a wide variety of applications including catalysis, sensors, actuators, fuel cells, microfluidic flow controllers, and so forth [1-4]. For a long time past, template methods are commonly used to fabricate these materials through the replication of porous alumina or liquid-crystal templates [5-7]. Since it has been found that dealloying can be used to yield a broad range of porous metals, during the latest decades, a great deal of effort has been directed towards the investigation of nanoporous metals prepared through dealloying [8-13]. However, most of the previously reported porous metals were

fabricated by dealloying from binary/ternary alloy systems with a single-phase solid solubility across all compositions, which refers to selective dissolution of one or more active components out of an alloy, such as Cu–Pt, Ag–Au, Cu–Au, and Au–Ag–Pt [14-17]. In view of their industrial applications, widespread uses of dealloying technique to make nanoporous metals are frequently hindered by the high cost of these noble metals and limited alloy systems. Thus, the fabrication of nanoporous materials from alloy families based on common metals with multiple phases urgently needs to be investigated.

However, no many substantial researches have so far focused on this topic using electrochemical/chemical dealloying technique because of the difficulties in clarifying dealloying behavior and controlling dissolution process among different phases in multi-phase alloys [18]. Recently, we found that phase constitution in initial alloys has a key effect on the dealloying behavior and dissolution process among multiple phases [19-20]. For example, compared to the NPC obtained from the Al 33 at.% Cu alloy consisting of single Al₂Cu intermetallics, the melt-spun Al 40 at.% Cu alloy comprising Al₂Cu and AlCu intermetallics just can be partially dealloyed and results in the formation of a unique kind of NPC/AlCu composites. According to the binary Al-Cu alloy phase diagram [21], it could be expected theoretically that the dealloying behavior and dissolution process among phases in the Al-Cu alloy comprising solid solutions and intermetallics might make an essential difference relative to counterpart completely composed of intermetallics, such as the previous Al 40 at.% Cu alloy, due to the large disparity in phase constitution of initial alloy.

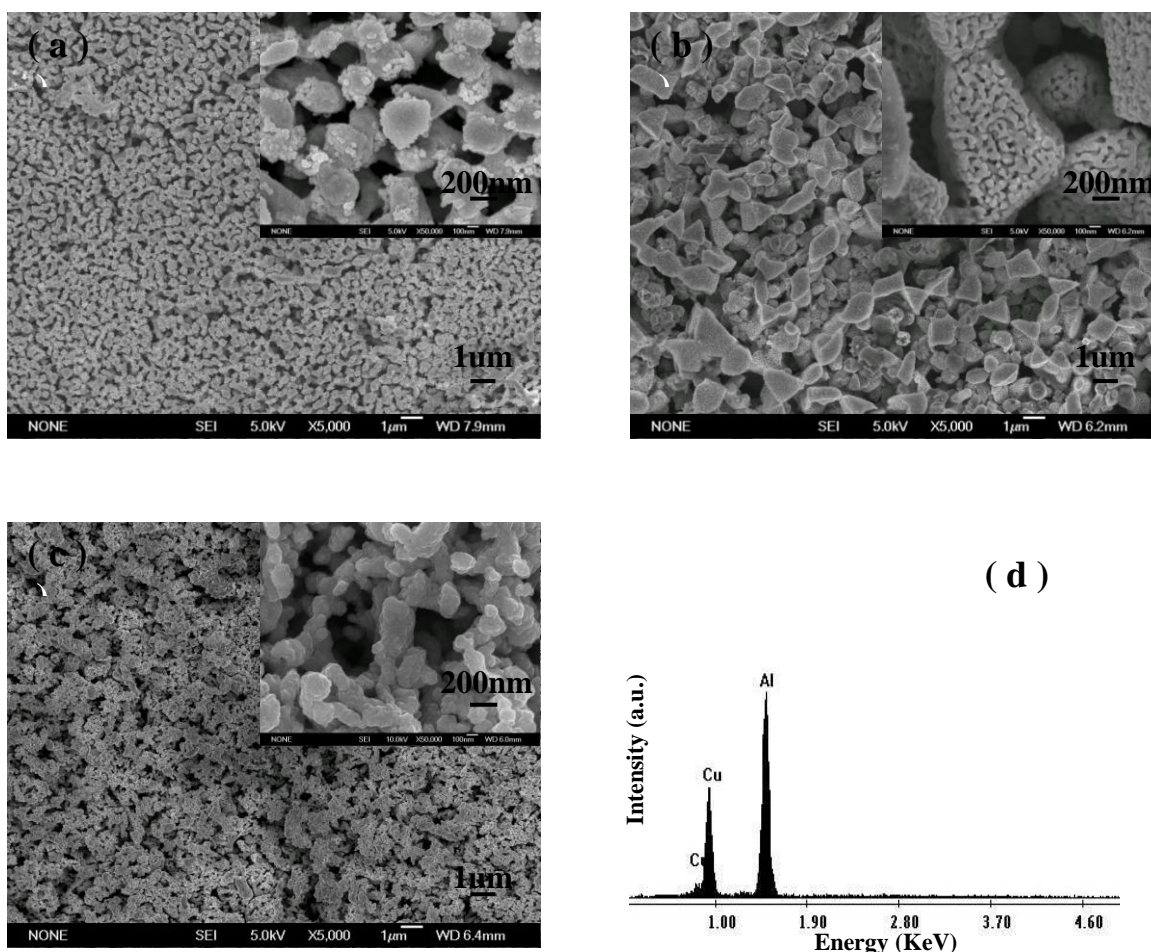
To test this idea, Al 15 at.% Cu alloy ribbons comprising α -Al solid solution and Al₂Cu intermetallic compound was taken as an example to investigate the dealloying behavior and dissolution process between phases during chemical dealloying process. The results show that the Al-Cu alloy with the amount of α -Al comparable to that of Al₂Cu can be completely dealloyed in the acidic solution, which eventually forms the NPC ribbons with a uniform porous structure, while during which two other kinds of nanoporous structures were sequentially obtained for different dealloying times. The morphological and compositional evolutions of the resultant porous products upon dealloying were studied, and their formation mechanism is discussed.

2. EXPERIMENTAL SECTION

Al-Cu alloy with nominal composition of 15 at.% Cu was prepared from pure Al (99.99 wt.%) and pure Cu (99.999 wt.%). Voltaic arc heating was employed to melt the charges in a copper crucible under an argon atmosphere, and then the melt was cooled down into ingots in situ. By use of a single roller melt spinning apparatus, the Al-Cu ingots were remelted in a quartz tube by high-frequency induction heating and then melt-spun onto a copper roller at a circumferential speed of ~3000 rpm in a controlled argon atmosphere. The ribbons obtained were typically 20-40 μ m in thickness, 4-6 mm in width, and several centimeters in length. The dealloying of the melt-spun Al-Cu alloy ribbons was performed in a 5 wt.% HCl aqueous solution at room temperature (RT) for different times, respectively. After dealloying, the samples were rinsed with distilled water and dehydrated alcohol. The as-dealloyed samples were kept in a vacuum chamber to avoid oxidation. Microstructural

characterization and analysis of the initial Al 15 at.% Cu alloy and as-dealloyed samples were made using X-ray diffraction (XRD, Rigaku D/Max-2400) with Cu K α radiation, scanning electron microscopy (FESEM, Hitachi S-4800) with an energy dispersive X-ray (EDX) analyzer, transmission electron microscopy (TEM, JEOL JEM 2100F) with selected-area electron diffraction (SAED). To test the electrochemical activities of α -Al and Al₂Cu phases in the melt-spun Al 15 at.% Cu alloy, potentiodynamic polarizations studies were conducted on single-phase α -Al solid solution and Al₂Cu intermetallic compound (corresponding to Al-Cu alloy with a trace amount of Cu and Al 33 at.% Cu alloy) in the 5 wt.% HCl solution at RT by using an electrochemical measurement unit (PARSTAT 2273). The experiments were carried out in a standard three-electrode electrochemical cell (200mL) with a Pt plate electrode as a counter electrode, a saturated calomel electrode (SCE) as a reference electrode, and the alloy ribbon as the working electrode. Polarization scan was performed towards positive values at a scan rate of 1.0 mV s⁻¹, after allowing a steady state potential to develop. In order to evaluate specific surface areas of the porous products, the N₂ adsorption/desorption experiments were carried out at 77 K on a Nova Station A automatic surface area and pore radius distribution apparatus.

3. RESULTS AND DISCUSSION



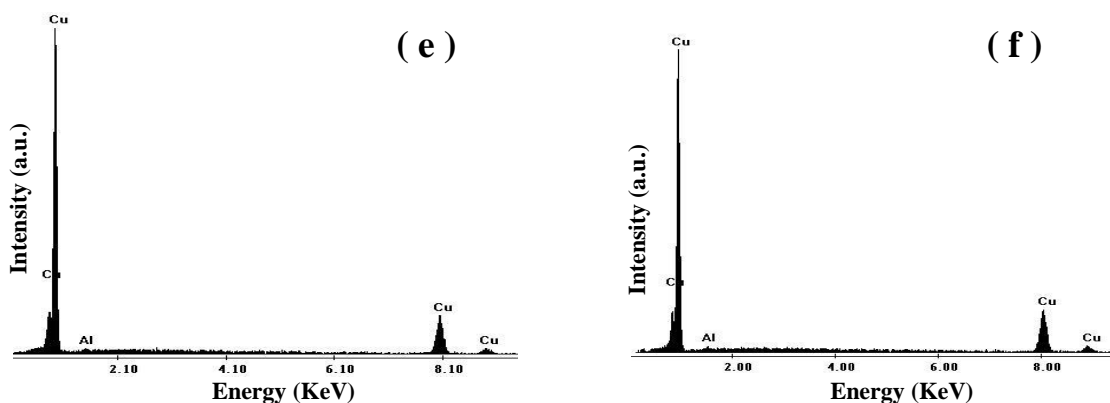


Figure 1. SEM images showing the microstructure of the as-dealloyed samples by dealloying of the Al 15 at.% Cu alloy in the 5 wt.% HCl solution at RT for (a) 4 h, (b) 10 h, (c) 96 h. Insets of parts a-c are the high-magnification images. (d-f) shows the EDX spectra of porous structures corresponding to parts a-c.

Figure 1 shows the microstructure of as-dealloyed samples upon dealloying for different times, respectively. When the dealloying time reaches 4 h, a uniform porous structure with length scales of 200-300 nm can be obtained in the as-dealloyed samples (Figure 1a). With the dealloying time up to 10 h, the sample surface exhibits a porous structure with length scales of 400-500 nm, and the SEM image at a higher magnification shows the pore walls exhibit an open, bicontinuous interpenetrating ligament-pore structure with length scales of 40-50 nm (Figure 1b). As a result, the porous structure is composed of interconnected large-sized pores with highly porous pore walls. As to the NPC ribbons upon dealloying for 96 h, its microstructure can be characterized by a three-dimensional bicontinuous network morphology with larger length scales of ligaments/pores (600-800 nm, Figure 1c).

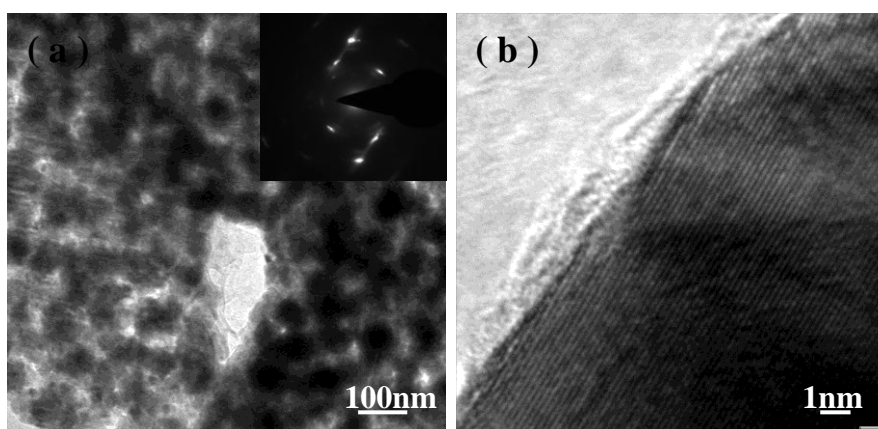


Figure 2. (a) TEM image showing the porous structure with bimodal pore size distributions of the NPC ribbons by dealloying of the Al 15 at.% Cu alloy in the 5 wt.% HCl solution at RT. (Inset) SAED pattern corresponding to one ligament in part a. (b) HRTEM image shows lattice fringes extending throughout the whole ligament in the pore walls.

EDX analysis has been performed on all the as-dealloyed samples, and typical spectra are shown in Figure 1d-f. Obviously, the uniform porous structure upon dealloying for 4 h is enriched in Al, and the atomic percentage of Al and Cu in the porous structure is close to 2:1, indicating the uniform nanoporous structure is Al_2Cu phase (Figure 1d), while nearly all of Al can be removed from the Al-Cu alloy upon dealloying over 10 h (Figure 1e-f). Herein, we define the uniform nanoporous structure composed of single Al_2Cu phase as NP- Al_2Cu , the NPC composed of interconnected large-sized pores with highly porous pore walls as bimodal NPC, and the NPC with a uniform porous structure as unimodal NPC.

TEM observation further verifies the porous structure of the bimodal NPC ribbons upon dealloying in the HCl solution for 10 h and one typical TEM bright-field image is shown in Figure 2a. The SAED pattern of one ligament in porous pore walls is from the face-centered cubic (f.c.c.) Cu [110] zone axis, indicating a single crystalline characteristic of the selected area (inset of Figure 2a). Moreover, lattice fringes extending throughout the whole ligament further verify the single crystal nature of the ligament in the pore walls (Figure 2b). It should be noted, however, the present results are essentially different from the established notion that the crystal lattice orientation is retained during dealloying of Ag-Au alloys with the conservation of the grain size of the master alloys [22-25]. For the Al-Cu alloy in this work is considerably different from the Ag-Au system due to their complex lattice structures (Al_2Cu : single body centered tetragonal; $\alpha\text{-Al}$: solid solution).

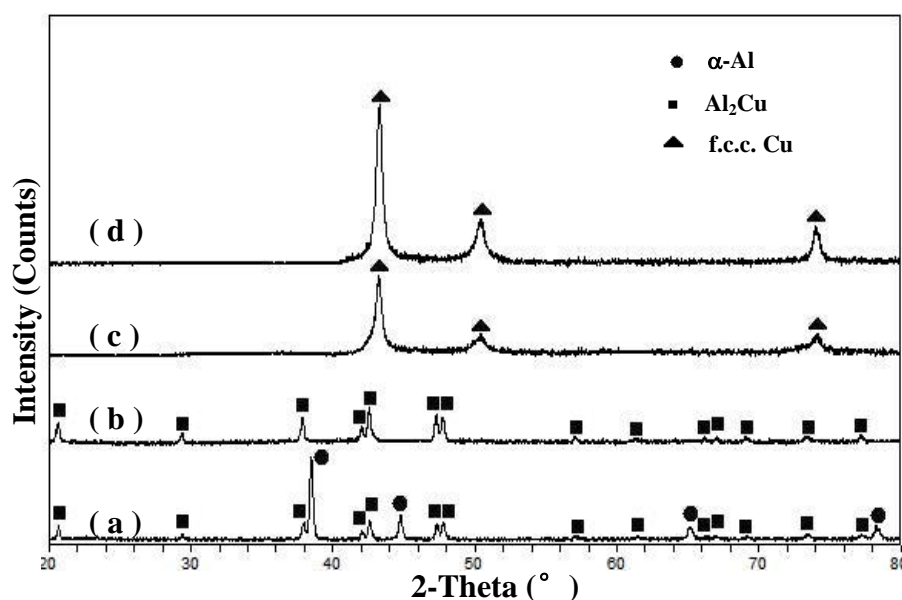


Figure 3. XRD patterns of melt-spun Al 15 at.% Cu alloy ribbon (a) before and (b-d) upon dealloying in the 5 wt.% HCl solution at RT for 4 h, 10 h, 96 h.

The melt-spun Al 15 at.% Cu alloy ribbons and as-dealloyed samples upon dealloying for different times are also characterized by X-ray diffraction, with typical patterns shown in Figure 3. The filled circles, squares and triangles stand for $\alpha\text{-Al}$, Al_2Cu and Cu, respectively. The initial Al 15 at.%

Cu alloy is composed of two phases: α -Al and Al_2Cu , in which the amount of α -Al is comparable to that of Al_2Cu . Upon dealloying for 4 h, single body centered tetragonal Al_2Cu can be detected in the as-dealloyed samples, confirming that the uniform porous structure is Al_2Cu phase, while only a f.c.c. Cu can be identified as the dealloying times over 10 h, demonstrating that the bimodal and unimodal porous structures are Cu phases.

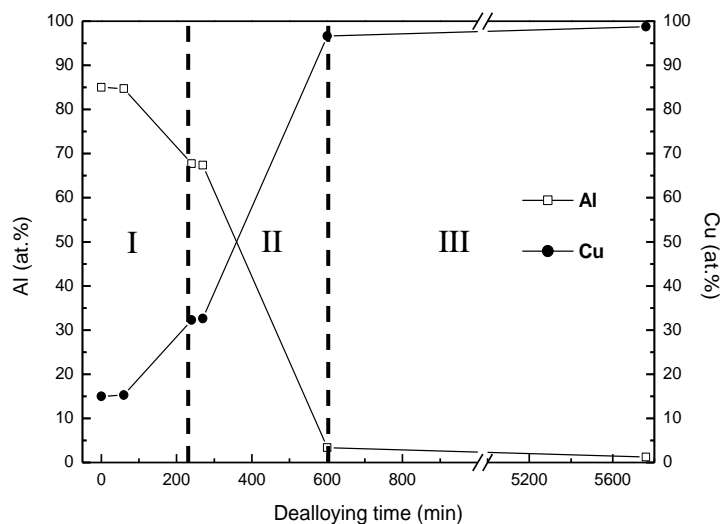


Figure 4. Composition evolution of the melt-spun Al 15 at.% Cu alloy ribbons with dealloying time at RT as measured by EDX. Region I, II and III denote three distinguishable composition regions, respectively.

Figure 4 shows the composition evolution of the melt-spun Al 15 at.% Cu alloy ribbons in the 5 wt.% HCl solution at RT with dealloying time as measured by EDX. With increasing dealloying time, three composition regions can be distinguished, which are denoted by region I, region II and region III, respectively. It can be seen from the region I that the atomic percentages of both Al and Cu first slightly change. This could correspond to the dissolution of surface Al atoms in α -Al, which is in line with the SEM observations shown in Figure S1 (Supporting Information). Subsequently, the composition altered dramatically when the dealloying time spans from 60 min to 240 min. The atomic percentage of Cu increased to 32.3%, while that of Al decreased down to 67.7%, which implied that dealloying took place in the volume of the alloy ribbons. This is also confirmed by the excavation of α -Al phase and the formation of porosity, as illustrated in Figure 1a. In region II, the composition of the porous samples experiences a similar variation process to the previous region I. Namely, it first varies slightly as long as the dealloying time does not exceed 270 min, and then the atomic percentage of Cu rose sharply, accompanied by a corresponding decrease in the content of Al until the dealloying time for 10 h. This suggests that the dealloying of Al_2Cu phase constituting pore walls in the NP- Al_2Cu ribbons also involves two processes of surface and interior dealloying. Thereafter, a slighter composition change can be observed in region III spanning a very long etching period, which is most likely related to the gradual exposure and re-dealloying of a trace amount of residual Al_2Cu inside

porous pore walls via the surface diffusion of Cu atoms. Note that the composition changed little, like a steady state, when the dealloying time up to 96 h. In contrast, when the melt-spun Al 15 at.% Cu alloy ribbons were dealloyed in the 5 wt.% HCl solution at 75°C, its compositional evolution with dealloying time is pronouncedly different from that at RT, especially no obvious quasi-plateau phase can be observed in region I and region II (Figure S2, Supporting Information). Thus, we can conclude that the temperature also plays a key role in the dealloying behavior and dissolution process of the dual-phase Al 15 at.% Cu alloy in the acidic solution.

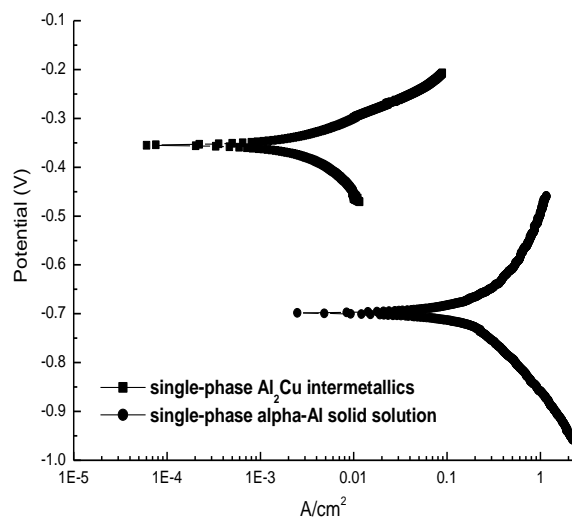


Figure 5. Tafel polarization curves of single-phase α -Al solid solution and Al₂Cu intermetallic compound in the 5 wt.% HCl solution at RT.

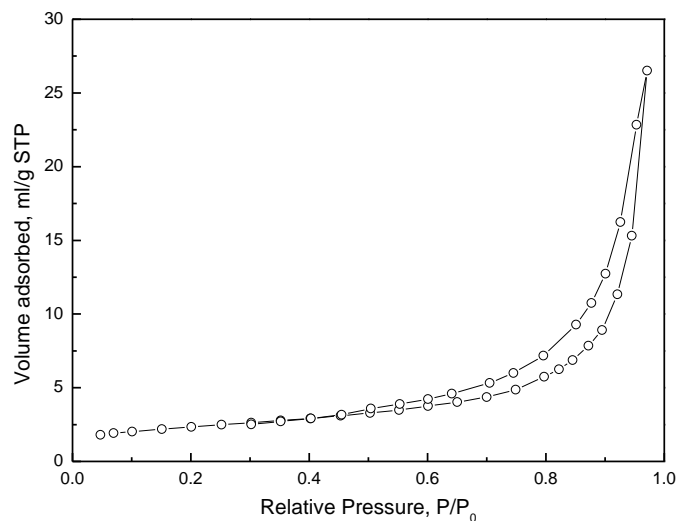


Figure 6. N₂ isotherm at 77 K for the bimodal NPC by dealloying of the melt-spun Al 15 at.% Cu alloy in the 5 wt.% HCl solution for 10 h.

Figure 5 shows Tafel polarization curves of single-phase α -Al solid solution and Al_2Cu intermetallic compound in the HCl solution at RT, respectively. It can be found that the difference between free-corrosion potentials of the single-phase α -Al and Al_2Cu in the acidic solution is ~ 343.1 mV(SCE), and the counterpart between corrosion currents of them is ~ 0.1508 A cm^{-2} , which clearly indicates that the α -Al have a relatively high electrochemical activity compared to the Al_2Cu in the HCl solution.

The specific surface areas of these porous samples can be evaluated based upon N_2 adsorption/desorption experiments. Figure 6 shows the N_2 adsorption/desorption isotherm for the bimodal NPC ribbons by dealloying of the melt-spun Al 15 at.% Cu alloy in the HCl solution for 10 h. The result shows that the Brunauer-Emmett-Teller (BET) surface area of the appointed samples is much high and has been determined to be 8.2 ± 0.1 m^2 g^{-1} . It is worthwhile noting that this interesting structural feature endows the NPC ribbons with higher surface area, which is especially beneficial for catalysis and sensing applications.

Consider a dual-phase alloy, A_pB_{1-p} , where a relatively large difference exists in the metal/metal-ion equilibrium potentials between A and B, and element A is more electroactive. A_xB_{1-x} and A_yB_{1-y} ($x > y$) denote as the two phases existing in the A_pB_{1-p} alloy. It can be presumed that both A_xB_{1-x} and A_yB_{1-y} phases meet the dealloying threshold, which makes the dealloying process in bulk A_pB_{1-p} alloy feasible. The different contents of A in A_xB_{1-x} and A_yB_{1-y} determines whether highly effective galvanic cells exist, and A_xB_{1-x} is an anodic phase, which corrodes preferentially, prior to spreading out in the A_yB_{1-y} phase. In this case, the present Al 15 at.% Cu alloy composed of α -Al and Al_2Cu phases. According to the binary Al-Cu alloy phase diagram [21], during the solidification of the alloy, eutectics of α -Al and Al_2Cu phases can directly nucleate and continually grow from the initial liquid, suppressing the precipitation of primary Al_2Cu phase due to the fast cooling rate, characteristic of an ideal two-phase bicontinuous microstructure (namely, quasieutectic structure). As indicated in Figure 5, the electrochemical activity of α -Al is much higher than that of Al_2Cu . Thus, α -Al and Al_2Cu phases existing in the alloy can form corrosion couple cells, with the α -Al phase (Al-rich phase) acting as an anode and preferentially dissolving compared to the Al_2Cu phase. The excavation of the α -Al phase from the bicontinuous microstructure during the etching can contribute to the formation of the interconnected large-sized pores in the resultant samples, like the case for production of porous glasses [26]. This is why the NP- Al_2Cu ribbons can be obtained first in the as-dealloyed samples upon the dealloying of the Al 15 at.% Cu alloy for 4 h.

Moreover, the XRD results exhibit nearly all of Al atoms in Al_2Cu phase can be removed from the Al 15 at.% Cu alloy during the further dealloying of the NP- Al_2Cu ribbons, which is consistent with the composition evolution. As a result, the bimodal and unimodal NPC ribbons can be sequentially achieved upon the formation of NP- Al_2Cu ribbons. We consider that their formation mechanism can be explained as follows based upon a combination of morphology and composition evolutions of these porous products. Figure 7 illustrates a typical schematic for morphological evolution of the dual-phase Al 15 at.% Cu alloy during dealloying. Before dealloying, the melt-spun Al 15 at.% Cu alloy is composed of α -Al and Al_2Cu phases, as shown in Figure 7a. With increasing dealloying time, the dealloying process can be divided into three stages, denoted by stage I, stage II and stage III, respectively. In stage I, the α -Al phase in Al-Cu alloy acting as an anode dissolved

preferentially. When the dealloying time reaches 4 h, the α -Al just can be totally excavated from the initial alloy, resulting into the formation of NP- Al_2Cu with a homogenous porous structure, which is in line with the SEM observations described above.

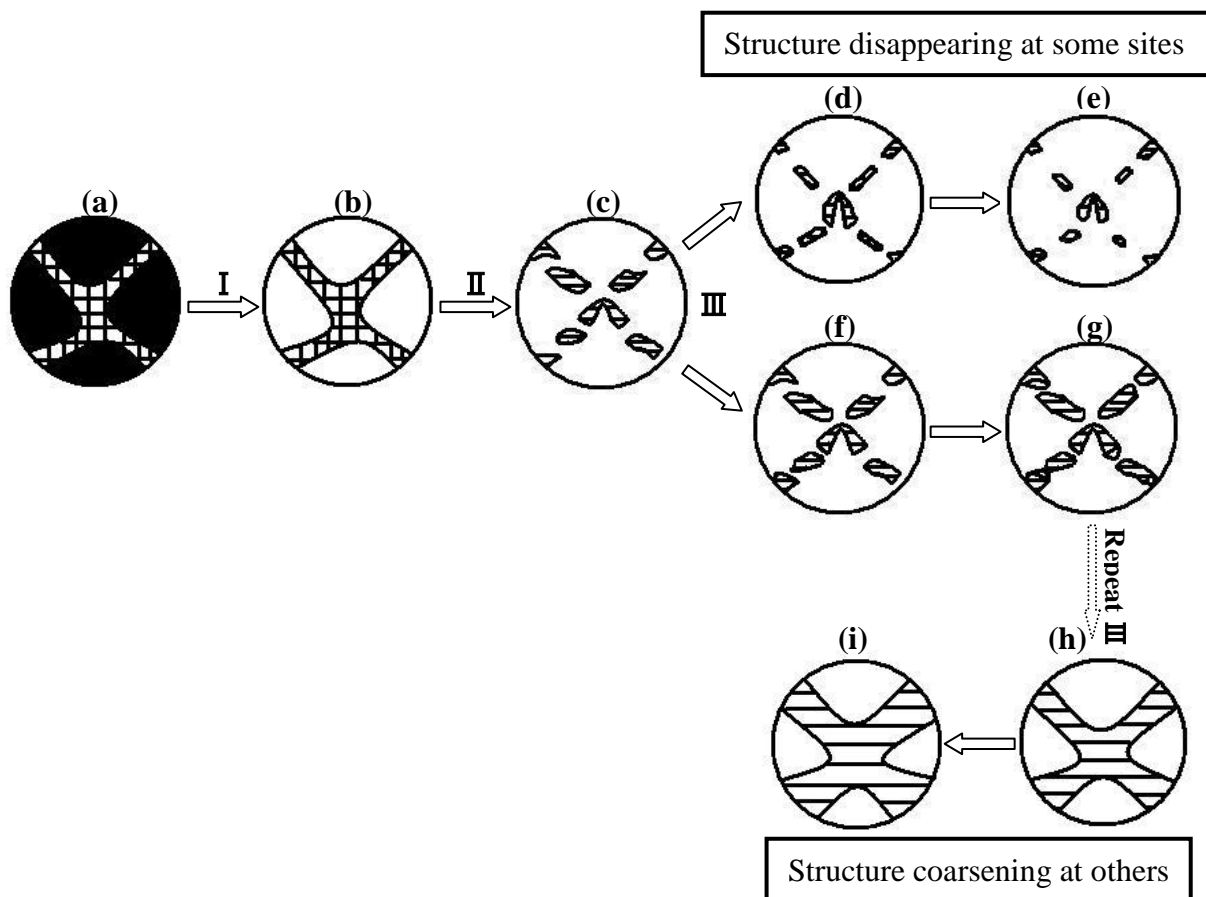


Figure 7. Schematic diagrams showing the dealloying process of the initial Al 15 at.% Cu alloy ribbons in the HCl solution: (a) pre-dealloying, (b-c) during dealloying, (d-i) post-dealloying. Stage I: “ α -Al dealloying”. Stage II: “ Al_2Cu dealloying”. Stage III: “coarsening of NPC in porous pore walls”.

Hence, stage I can be identified as “dealloying of α -Al” involving two processes of surface and interior dealloying of α -Al, corresponding to the initial two alteration processes of atomic percentages of both Al and Cu in region I of Figure 4. In stage II, Al_2Cu phase constituting pore walls in the NP- Al_2Cu ribbons begins to be etched and gradually evolves into the nanoporous structure in the pore walls. Typically, the Al atoms in Al_2Cu continuously dissolves into the solution and the remaining Cu atoms will reassemble to form the porous network through surface diffusion along the alloy/solution interfaces. When the dealloying time reaches 10 h, Al_2Cu phase can be completely dealloyed and results in the formation of bimodal NPC ribbons, in which large-sized pores resulting from entire dissolution of previous α -Al while small-sized those deriving from part corrosion of Al_2Cu . Thus, it could be defined as “ Al_2Cu dealloying” stage also containing two processes of surface and interior

dealloying of Al_2Cu phase, corresponding to the broken-line-typed composition evolution in region II of Figure 4 spanning dealloying time from 4 h to 10 h. In stage III, the porous structure of the bimodal NPC ribbons gradually coarsens due to the Ostwald ripening effects [27], which is kinetically controlled by the diffusion-rearrangement of Cu atoms in comparison with that essentially controlled by the dissolution of Al atoms in the first two stages. It should be noted that, however, the coarsening rate of the different-sized porous structures in the NPC ribbons is markedly different, in which the nanoporous structure in the pore walls can coarsen faster via surface diffusion of Cu atoms to minimize its total surface energy. In particular, diffusion and rearrangement of Cu atoms in porous pore walls can result in gradual disappearance of some porous structures, accompanied by slow coarsening of others during dealloying. Finally, the NPC ribbons with a uniform porous structure can be formed after the complete disappearance of nano-scaled ligament-pore structure in the pore walls. This stage could be designated as “coarsening of NPC in porous pore walls”, corresponding to the slighter composition variation in region III of Figure 4 as the dealloying time exceeds 10 h. It should be noted that the atomic percentage of Cu still rise slowly, accompanied by a corresponding decrease in the content of Al; eventually, a quasi-stable state can be achieved with the dealloying time up to 96 h. This is most likely related to the synergistic effect between low surface diffusivity of Cu atoms along alloy/solution interfaces and low residual Al_2Cu content in porous pore walls at this moment. The above-described mechanism may lead to the case that α -Al and Al_2Cu can be orderly dealloyed in the Al 15 at.% Cu alloy and holds accountable for the sequential formations of NP- Al_2Cu , bimodal and unimodal NPC ribbons.

In order to tentatively explore the underlying physical nature of dealloying of intermetallics, the dealloying of Al_2Cu phase in the melt-spun Al 15 at.% Cu alloy was preliminarily investigated. Figure S3 (Supporting Information) shows the representative TEM images of transition-state microstructure of Al_2Cu phase in the Al 15 at.% Cu alloy during dealloying process. The samples upon dealloying for 4.5 h exhibit a kind of mixed structure composed of cotton-like structure and porous structure, as presented in the high-magnification TEM images, respectively. The SAED pattern of porous structure consists of polycrystalline rings, corresponding to f.c.c. $(111)_{\text{Cu}}$, $(200)_{\text{Cu}}$, $(220)_{\text{Cu}}$, and $(311)_{\text{Cu}}$ reflections (inset of Figure S3c), while the counterpart of cotton-like structure is characteristic of light halo rather than diffraction rings or spots, indicating an amorphous nature of the selected area (inset of Figure S3b). The present experimental results demonstrate that a ‘crystal transfer’ process, from crystal to non-crystal and to crystal again, could exist in the dealloying process of the Al_2Cu , implying that the crystal nucleation and formation/removal of lattice sites should be necessary during the dealloying of intermetallics. In contrast, Parida and co-workers [24] have reported that the dealloying of prototypical Ag-Au solid solution system, such as $\text{Ag}_{70}\text{Au}_{30}$, does not require either nucleation of new crystallites or formation/removal of lattice sites. Thus, the result demonstrates that the dealloying mechanism of intermetallics is much more complicated than that of solid solution alloys reported in the previous studies. Recently, Zhang et al. [28] also have inferred that a more complicated mechanism, e.g., nucleation and growth instead of spinodal decomposition, is required for the Au atoms in the initial monoclinic AlAu lattice to reconstruct the f.c.c. structure of Au. It should be noted that, however, this is the first time to provide an experimental proof straightforwardly, indicating the

study on the underlying physical nature of dealloying of intermetallics takes a step forward from hypothesis.

Based on the present work, we are confident that it will have important implications for understanding the underlying physical mechanism of dealloying of multi-phase alloys, fabricating and tailoring the porous materials with different ligament-pore structures via controlling the dissolution processes among different phases, and thus lays a solid foundation for their promising applications in lithium ion batteries within the green, new energy industry. Some encouraging test findings have been obtained in our previous work [29-30], the extensive study is in progress.

4. CONCLUSION

The dual-phase Al 15 at.% Cu alloy with the amount of α -Al comparable to that of Al_2Cu can be totally dealloyed in the acidic solution, which results in the sequential formations of NP- Al_2Cu , bimodal and unimodal NPC ribbons. Their formation mechanism can be explained as a consequence of kinetic competitions between dissolution of Al atoms and diffusion-rearrangement of Cu atoms. Based on their dealloying behavior, an evolution law has been established, which includes three stages orderly described as “ α -Al dealloying,” “ Al_2Cu dealloying,” and “coarsening of NPC in porous pore walls.”

SUPPLEMENTARY DATA

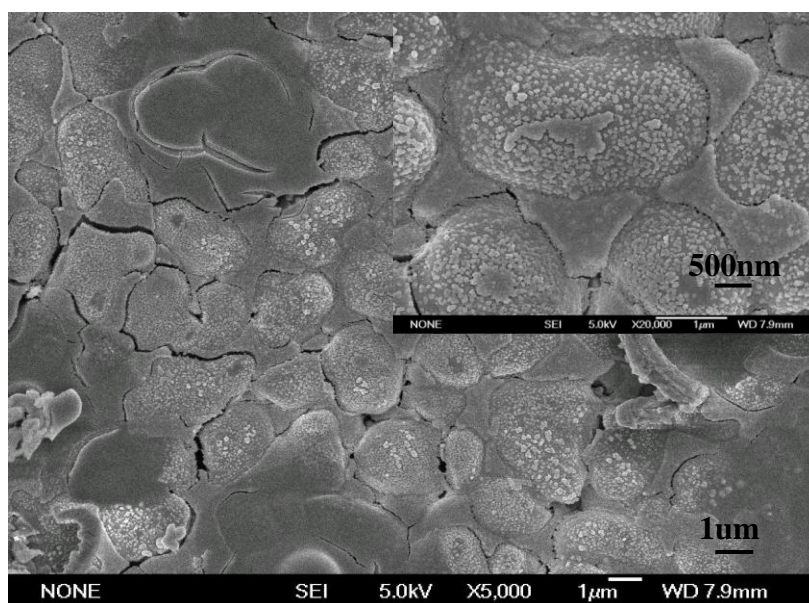


Figure S1. SEM images showing the microstructure of the as-dealloyed samples by dealloying of the melt-spun Al 15 at.% Cu alloy in the 5 wt.% HCl solution at RT for 1 h. Inset is the corresponding high-magnification image.

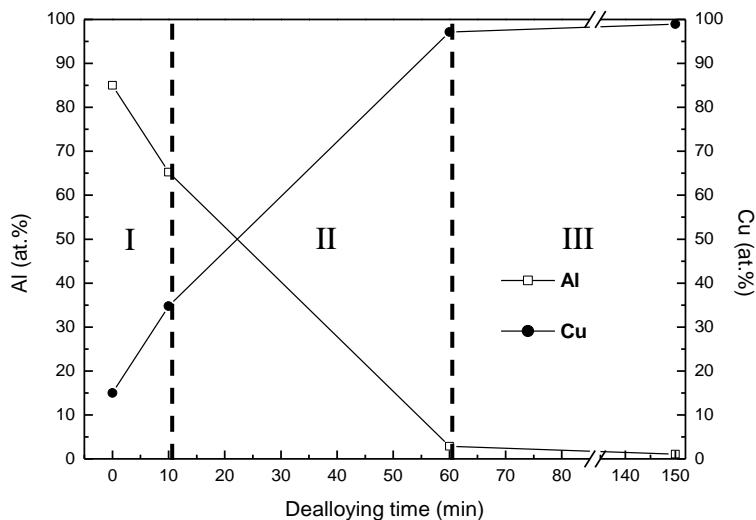


Figure S2. Composition evolution of the melt-spun Al 15 at.% Cu alloy ribbons with dealloying time at 75 °C as measured by EDX.

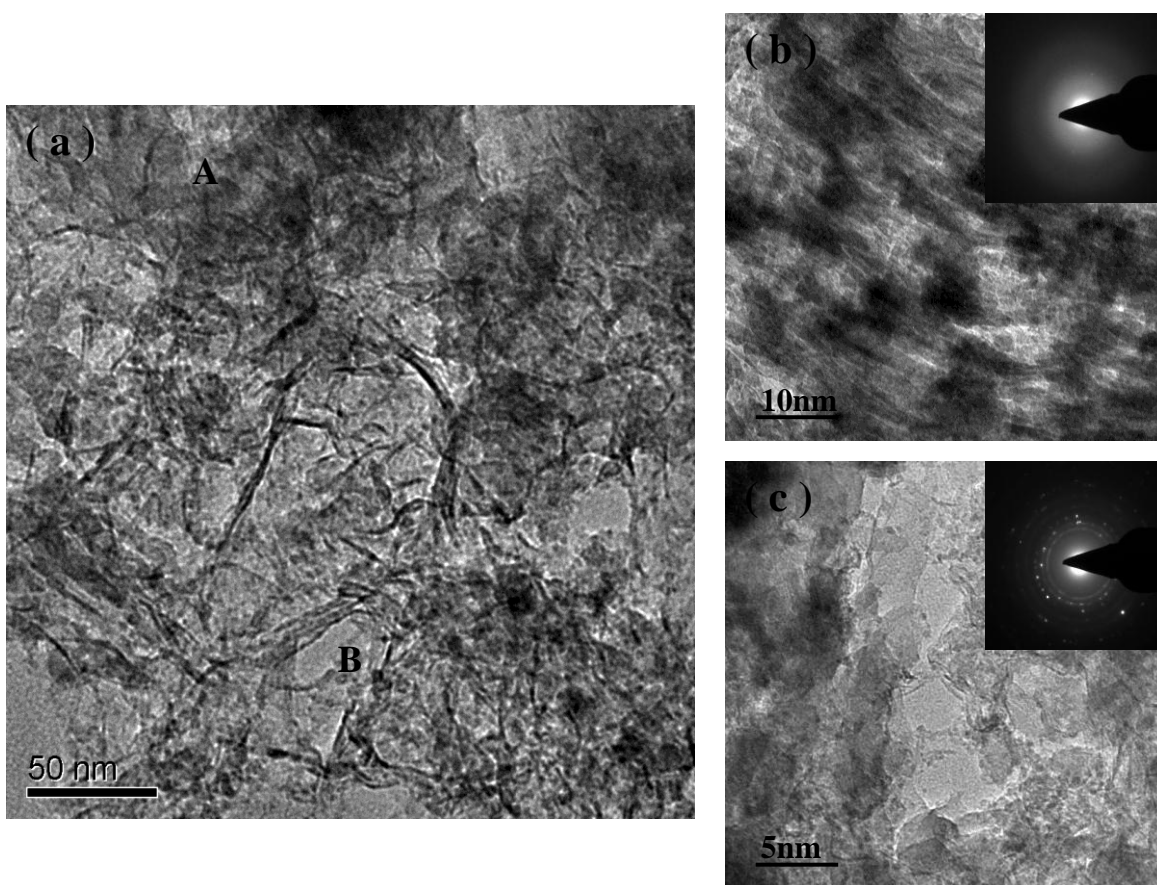


Figure S3. (a) TEM image showing the transition-state microstructure by dealloying of the Al₂Cu phase in the Al 15 at.% Cu alloy in the 5 wt.% HCl solution at RT for 4.5 h. Parts b and c are the high-magnification images corresponding to A and B sites marked in part a. Insets of parts b and c are the corresponding SAED patterns.

ACKNOWLEDGEMENT

We give thanks to financial support by the State Key Basic Research Program of PRC (2007CB936502), the National Natural Science Foundation of China (50574008, 50954005, 51074011), the National 863 Program Project (2006AA03Z230, 2008AA03Z208), and the China Postdoctoral Science Foundation Funded Project (2011M500214). Also, we are grateful to Prof. T. Zhang and Dr. J.F. Wang for assistance in preparation of the starting alloy ribbons.

References

1. G. C. Bond and D. T. Thompson, *Catal. Rev.*, 41 (1999) 319.
2. T. You, O. Niwa, M. Tomita and S. Hirono, *Anal. Chem.*, 75 (2003) 2080.
3. J. R. Weismueller, N. Viswanath, D. Kramer, P. Zimmer, R. Wuerschum and H. Gleiter, *Science*, 300 (2003) 312.
4. S. H. Joo, S. J. Choi, K. J. Kwa and Z. Liu, *Nature*, 412 (2001) 169.
5. H. Masuda and K. Fukuda, *Science*, 268 (1995) 1466.
6. G. S. Attard, P. N. Bartlett, N. R. B. Coleman, J. M. Elliott, J. R. Owen and J. H. Wang, *Science*, 278 (1997) 838.
7. T. Kijima, T. Yoshimura, M. Uota, T. Ikeda, D. Fujikawa, S. Mouri and S. Uoyama, *Angew. Chem., Int. Ed.*, 43 (2004) 228.
8. J. Erlebacher, M. J. Aziz, A. Karma, N. Dimitrov and K. Sieradzki, *Nature*, 410 (2001) 450.
9. K. Sieradzki, N. Dimitrov, D. Movrin, C. McCall, N. Vasiljevic and J. Erlebacher, *J. Electrochem. Soc.*, 149 (2002) B370.
10. C. X. Ji and P. C. Searson, *J. Phys. Chem. B*, 107 (2003) 4494.
11. M. Stratmann and M. Rohwerder, *Nature*, 410 (2001) 420.
12. W. B. Liu, S. C. Zhang, N. Li, J. W. Zheng and Y. L. Xing, *Microporous Mesoporous Mater.*, 138 (2011) 1.
13. W. B. Liu, S. C. Zhang, N. Li, J. W. Zheng, S. S. An and Y. L. Xing, *Int. J. Electrochem. Sci.*, 6 (2011) 5445.
14. D. V. Pugh, A. Dursun and S. G. Corcoran, *J. Electrochem. Soc.*, 152 (2005) B455.
15. U. S. Min and J. C. M. Li, *J. Mater. Res.*, 9 (1994) 2878.
16. B. W. Parks Jr., J. D. Fritz and H. W. Pickering, *Scripta Mater.*, 23 (1989) 951.
17. J. Snyder, P. Asanithi, A. B. Dalton and J. Erlebacher, *Adv. Mater.*, 20 (2008) 4883.
18. A. Dursun, D. V. Pugh and S. G. Corcoran, *J. Electrochem. Soc.*, 152 (2005) B65.
19. W. B. Liu, S. C. Zhang, N. Li, J. W. Zheng and Y. L. Xing, *Corrosion Sci.*, 53 (2011) 809.
20. W. B. Liu, S. C. Zhang, N. Li, J. W. Zheng and Y. L. Xing, *J. Electrochem. Soc.*, 158 (2011) D91.
21. T. B. Massalski, J. L. Murray, L. H. Bennett and H. Baker, *Binary Alloy Phase Diagrams*, American Society for Metals, Ohio, 1986.
22. Y. Ding, A. Mathur, M. W. Chen and J. Erlebacher, *Angew. Chem., Int. Ed.*, 44 (2005) 4002.
23. Y. Ding, Y. J. Kim and J. Erlebacher, *Adv. Mater.*, 16 (2004) 1897.
24. S. Parida, D. Kramer, C. A. Volkert, H. Rössner, J. Erlebacher and J. Weismüller, *Phys. Rev. Lett.*, 97 (2006) 035504.
25. A.J. Forty and P. Durkin, *Philos. Mag. A*, 42 (1980) 295.
26. D. Enke, F. Janowski and W. Schwieger, *Microporous Mesoporous Mater.*, 60 (2003) 19.
27. A.M. Hodge, J. Biener, J. R. Hayes, P. M. Bythrow, C. A. Volkert and A. V. Hamza, *Acta Mater.*, 55 (2007) 1343.
28. Q. Zhang, X. G. Wang, Z. Qi, Y. Wang and Z. H. Zhang, *Electrochimica Acta*, 54 (2009) 6190.
29. S. C. Zhang, Y. L. Xing, W. B. Liu and J. W. Zheng, *The 15th International Meeting on Lithium Batteries, IMLB*, J. Electrochem. Soc., Abstract #82, Montréal, Canada, June 27-July 2, 2010.

30. W. B. Liu, S. C. Zhang, J. W. Zheng and Y. L. Xing, *The 4th international conference on advanced lithium batteries for automobile application, ABAA-4*, Tianjin Institute of Power Sources & China Industrial Association of Power Sources, Abstract #108, Beijing, China, September 21-23, 2011.